Imaging of prostate cancer: a platform for 3D co-registration of in-vivo MRI ex-vivo MRI and pathology

Clement Orczyk[1ab], Artem Mikheev [b], Andrew Rosenkrantz [b], Jonathan Melamed [b], Samir S. Taneja [b], Henry Rusinek [b]
[a]University Hospital of Caen, Avenue de la Côte de Nacre, Caen FRANCE 14033
[b]New York University Medical Center. 550 1st Avenue, New York NY USA 10016

ABSTRACT

Objectives: Multi-parametric MRI is emerging as a promising method for prostate cancer diagnosis. prognosis and treatment planning. However, the localization of in-vivo detected lesions and pathologic sites of cancer remains a significant challenge. To overcome this limitation we have developed and tested a system for co-registration of in-vivo MRI, ex-vivo MRI and histology.
Materials and Methods: Three men diagnosed with localized prostate cancer (ages 54-72, PSA levels 5.1-7.7 ng/ml) were prospectively enrolled in this study. All patients underwent 3T multi-parametric MRI that included T2W, DCE-MRI, and DWI prior to robotic-assisted prostatectomy. Ex-vivo multi-parametric MRI was performed on fresh prostate specimen. Excised prostates were then sliced at regular intervals and photographed both before and after fixation. Slices were perpendicular to the main axis of the posterior capsule, i.e., along the direction of the rectal wall. Guided by the location of the urethra, 2D digital images were assembled into 3D models. Cancer foci, extra-capsular extensions and zonal margins were delineated by the pathologist and included in 3D histology data. A locally-developed software was applied to register in-vivo, ex-vivo and histology using an over-determined set of anatomical landmarks placed in anterior fibro-muscular stroma, central. transition and peripheral zones. The mean root square distance across corresponding control points was used to assess co-registration error.
Results: Two specimens were pT3a and one pT2b (negative margin) at pathology. The software successfully fused in-vivo MRI. ex-vivo MRI fresh specimen and histology using appropriate (rigid and affine) transformation models with mean square error of 1.59 mm. Coregistration accuracy was confirmed by multi-modality viewing using operator-guided variable transparency.
Conclusion: The method enables successful co-registration of pre-operative MRI, ex-vivo MRI and pathology and it provides initial evidence of feasibility of MRI-guided surgical planning.

Keywords: prostate cancer. co-registration, MRI, histology, surgical planning, human studies, focal therapy

1. INTRODUCTION

In vivo magnetic resonance imaging (MRI) has evolved as the most promising noninvasive modality for visualizing prostate anatomy and for detecting tumors. With improvement in MRI hardware and sequences there is an increasing realization of a potential of multiparametric MRI (mpMRI) to characterize prostate tissue [1]. MpMRI combines the superb high-resolution anatomic visualization with quantitative assessment of tissue T1 and T2 relaxation rates, regional perfusion and diffusion characteristics, and, the measurements choline and citrate concentration using magnetic resonance spectroscopy. This synergetic conjunction of anatomical and functional parameters has demonstrated high sentivity and specificity of mpMRI for detection and characterization of prostate cancer in peripheral zone and central gland [234]. Managing and follow-up of prostate cancer is also emerging as promising clinical application for mpMRI [56].

In addition mpMRI is a key imaging modality in surgical procedure planning, guidance and evaluation. This includes planning for focal therapy for prostate cancer, a concept under evaluation in several clinical trials. Focal therapies

[1] clement.orczyk@yahoo.fr; phone number + 33 6 22 48 26 44

Medical Imaging 2012: Image-Guided Procedures, Robotic Interventions, and Modeling,
edited by David R. Holmes III, Kenneth H. Wong, Proc. of SPIE Vol. 8316, 83162M

currently available include: interstitial laser ablation, radiofrequency ablation, dynamic phototherapy, cryotherapy. and high-intensity focused ultrasound [7]. Current trials require mpMRI to define a target cancerous lesion in a 3D space.

Careful assessment of accuracy and comprehensive validation process is needed to translate mpMRI to wider patient care. This means that the MRI findings have to be confirmed with histology findings. Surgical resection of the entire prostate or radical prostatectomy (RP) is the standard curative therapy for prostate cancer. RP is performed in tens of thousands men per year. Until recently this approach was the basic treatment for prostate cancer and a large fraction of newly diagnosed cancers with high risk features [8] is still treated with RP to cure organ-confined disease.

Radical prostatectomy yields the gross surgical specimen and gives us the opportunity for detailed histological evaluation. Resected specimen is sliced to allow pathology assessment that is the gold standard for cancer diagnosis, prognosis, tissue characterization and pathological surgical staging. Pathology slides allow a detailed exam of the prostate tissue under optical microscopy and establishment of the Gleason score for prostate cancer. The distinction of tumors with Gleason score of 6 from Gleason score 7 and higher is critical for accurate prognostic determinations. Cancers with Gleason score of 6 are characterized by the preservation of discrete glandular units. Higher Gleason score tumors have characteristic microacinar glands, poorly formed lumina, large cribriform glands and cribriform glands with irregular borders. In the most advanced cases the tumor shows essentially an absence of glandular differentiation, with solid sheets of malignant cells.

In addition to loss of connective tissue and blood from vasculature there are also potential shape differences between resected specimen and in vivo prostate. The surgical procedure is known to modify the tissue shape and it introduces three-dimensional changes in size [9]. Formalin fixation and paraffin embedding induce variable tissue shrinkage [910]. Deformation of tissue and shredding artifacts are also common [11].

The problem of spatial alignment of in-vivo images and resected specimen is of intense interest. Mazaheri et al. [12] developed a methodology to co-register histology sections with T2W MR acquired using an endorectal coil. This approach used a deformable algorithm and the method of moments, and reported good accuracy. Chappelow et al. [13] developed a process based on mutual information to co-register mpMRI and histology in two-dimensions. Xiao et al [14] has also studied the problem of correspondence between T2-weighted images of the prostate and histology sections and have established good correlation between the automated procedure and expert findings. However their process is also restricted to 2D and assumes that histology and MR slices are in the same plane and have the same thickness.

There is therefore an important need to extend co-registration of mpMRI, surgical specimen and histology to full 3 dimensions. Such methodology will open the possibility of accurate advanced assessment of various aspects of MRI signature of detected disease, including image texture and heterogeneity. 3D correspondence is also essential for the application of mpMRI to guide focal therapy. Tissue boundaries and tumor margins can be evaluated with such methodology for improved surgical and oncological success.

The current study addresses co-registration of in-vivo MRI, ex-vivo MRI, 3D rebuilt surgical specimen and histologic sections. Since the prostate is an organ particularity rich in anatomical features, its well-systematized zonal anatomy combined with high spatial resolution of prostate images offers the possibility of designating numerous anatomical landmarks. Our approach will rely on the ability of the expert to identify corresponding points, independent of cancer. We use non–rigid transformation in order to obtain quantitative spatial correlation in spite of volume changes that occur during slicing process. Our objective was to design and validate a systematic workflow that leads to an accurate transformation between in vivo prostate captured by MRI and histology.

2. MATERIALS AND METHODS

2.1. Patients

Patient eligibility for this study included: having localized prostate cancer diagnosed with needle biopsy and being scheduled for robot-assisted radical prostatectomy. Three patients were prospectively enrolled in this study according to an IRB approved protocol. Informed consent was obtained for each study subject.

2.2. In vivo MRI

We acquired in vivo MRI on a 3T system (Magnetom Trio. Siemens Healthcare) with pelvic phase array coil and without endorectal coil. The imaging sequences included:

High-resolution anatomical T1-weighted sequence: axial images through the prostate and seminal vesicles: repetition time (TR) = 3208 ms, echo time (TE) 86 ms, 720 x 720 x 25 acquisition matrix, no interslice gap, 0.3 x 0.3 x 4.0 mm^3 voxel size. 2 signal averages.

Anatomical T2-weighted sequence: acquired in axial orientation using the same slice locations as T1-weighted imaging. The parameters for this turbospin-echo sequence were: TR = 4950 ms, TE = 122 ms, 256 x 256 x 25 acquisition matrix, no interslice gap, 1 x 1 x 4 mm^3 voxel size, 3 signal averages.

Diffusion weighted sequence: axial fat-suppressed single shot echoplanar images through the pelvis: TR=4600 ms. TE=75 ms. diffusion gradient b-values of 0 and 1000 s/mm^2. slice thickness 4 mm. 128 x 128 matrix. 7 signal averages. ADC maps were reconstructed inline.

Dynamic contrast-enhanced MRI. T1-weighted 3 mm thick contiguous images were acquired every 30 sec after IV administration of 10 ml gadolinium chelate. Contrast was injected using a power injector.

2.3. Robot assisted prostatectomy

Laparoscopic robotic assisted prostatectomy was performed with the assistance of a surgical robot (da Vinci system,. Sunnyvale CA USA). This procedure duplicates the standard open surgical radical retropubic rostatectomy (RRP) but with smaller incisions. Instead of the midline incision extending up from the pubic bone towards the umbilicus (as for the open surgical procedure), five small incisions (one-quarter to one-half inch each) are made in the lower abdomen. Through these incisions are passed the robot-controlled video camera, two manipulating wrist-like arms that allow very fine movements, and two assisting instruments. Through the console the surgeon manipulates the robot arms and directs the camera with hand-controls while looking at the operative field with an immersive 3-dimensional view.

2.4. Ex vivo MRI technique

We acquired ex vivo MRI within 12 hours after radical prostatectomy and before sectioning. The excised prostate was embedded in a paraffin block. We have attempted to maintain the orientation to keep the posterior capsule perpendicular to the plane of slicing. The orientation of MR scan is the same as the in vivo procedure. This procedure facilitates the identification of corresponding features between MRI and histology. MR imaging followed the same anatomical protocol as for in vivo system, including T1-weighted and T2-weighted sequences.

2.5. Pathology and histology processing

After radical prostatectomy and ex-vivo MRI the specimen was inked for margin and lateral side identification. When present, the seminal vesicles were transecting at the base and the weight of the prostate gland was determined. Pathologic workup was performed according to a modified Stanford protocol and included the measurement of the largest extents of the specimen in anterior-posterior, cranio-caudal, and left-right directions [15].

Since the posterior capsule is adjacent to the rectal wall, its plane was used as the reference for specimen slicing as well as for acquiring MRI data. The fresh gross specimen was sliced in contiguous parallel slices perpendicular to the posterior capsule from apex to bladder neck. The thickness of each slice was 4 mm. The number of slices depended on the total length of the gland. All slices were digitally photographed after placing them on a dedicated platform that provided a linear scale indication. The resolution of the digital camera was 210 pixels per cm. and the matrix size was 1024 x 1366.

A standardized fixation process in a formalin bath was applied next, with additional formalin injected in each slice. For histological sections, a single standard glass slide is too small to mount the entire slice, necessitating the cutting of the section into smaller fragments and mounting them onto multiple slides. Additionally. extremely thin (few microns) tissue samples are required for histology staining. Generating such thin specimen is difficult to achieve from an extended slice without tearing damage. Due to these challenges, it is preferable to cut large tissue specimens into smaller fragments and preparing multiple slides for separate analysis. Accordingly, after fixation each slice was cut in quadrants using two

perpendicular cuts, one in anterior-posterior direction, another left-to-right. After paraffin embedding 3-4 micron slides were cut and stained with hematoxylin and eosin. Stained histology slides were photographed using Canon camera (Canoscan 9000F), generating digital images resolved at 1200 pixels/inch. The four corresponding quadrants were then rebuilt into an image of the gross slice by border alignment using Photoshop CS5 software (Adobe Systems Inc, San Jose CA).

2.6. Three-dimensional reconstruction of photographed slices

The assembly of digital photographs of gross specimen slices into a 3D model relied on the McNeal's prostate zonal anatomy [16], with particular emphasis on urethral angulation. After assuring that digital images of each gross slice is adjusted to the same scale and the same field of view, the gland was segmented from background using Photoshop CS5. Segmented slices were translated to align urethra axis and posterior capsule. The inter-slice distance was assigned the original thickness determined during the slicing of surgical specimen and the entire image stack was then transformed in a 3D object using Image J software (V 1.44e, NIH). The output file was saved in a basic Analyze 7.5 raster file format (http://eeg.sourceforge.net/ANALYZE75.pdf). The resulting 3D dataset can now be manipulated and registered to MRI image. Note that the reconstruction of photographed ex-vivo slices is done independently of MRI findings.

2.7. Computation of co-registration transformation

Using locally developed software (https://files.nyu.edu/hr18/public/) we have performed landmark-based spatial registration between the three different modalities. We chose the T2-weighted sequence as the representative in vivo MRI for the process because the excellent anatomic resolution provided by this sequence permits reliable identification of anatomic landmarks.

A combination of the following eight 3D landmarks (Figs 1 and 2) were extracted based on the zonal anatomy of the gland:

Distal point of urethra at the apex
Veru montanum
Anterior-most point of the peripheral zone horn
Left ejaculatory duct
Right ejaculatory duct
Anterior-most point of the gland overall
Proximal end of urethra at the prostate base, adjacent to the bladder
Posterior junction of peripheral zone and transition zone overall

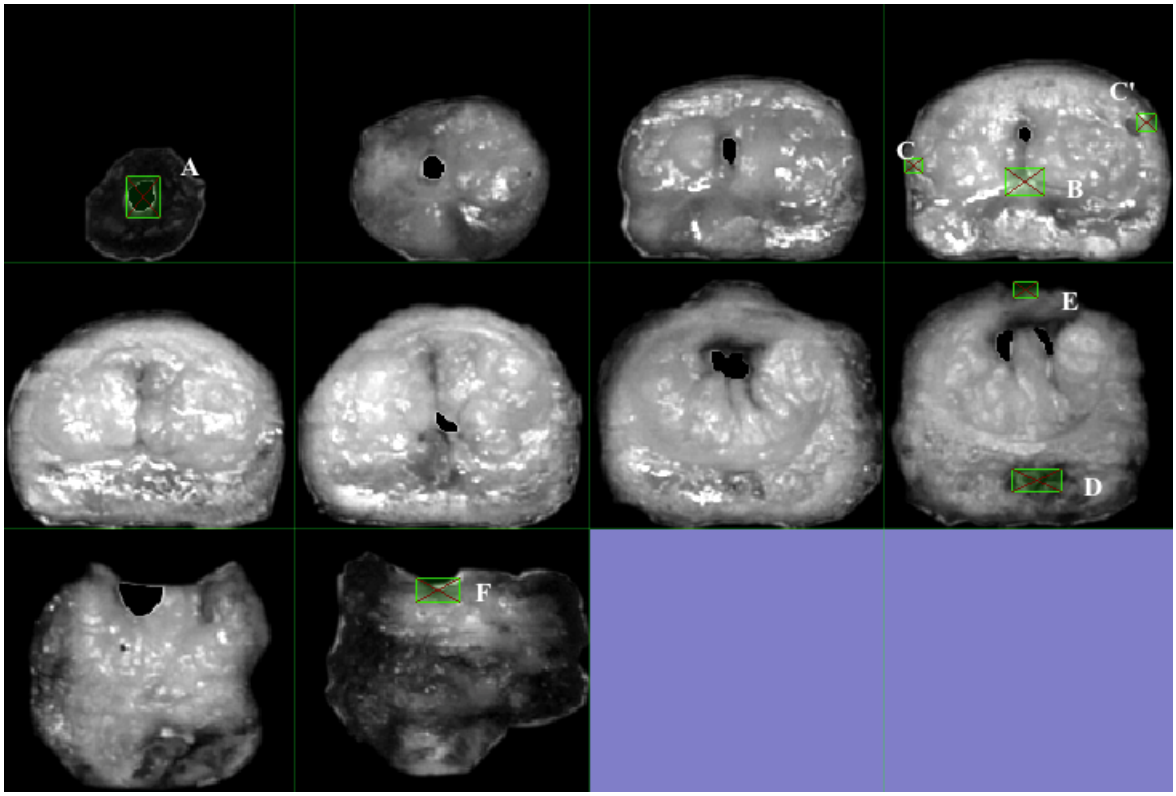

Figure 1. Surgical specimen with registration landmarks in axial plane

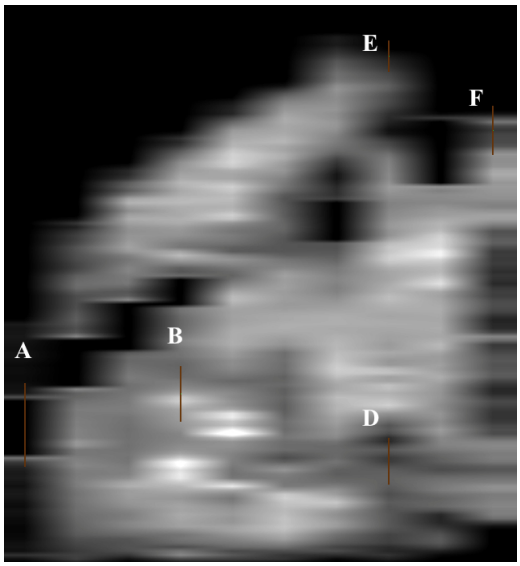

Figure 2. Surgical specimen in 3D with registration landmarks − sagittal plane

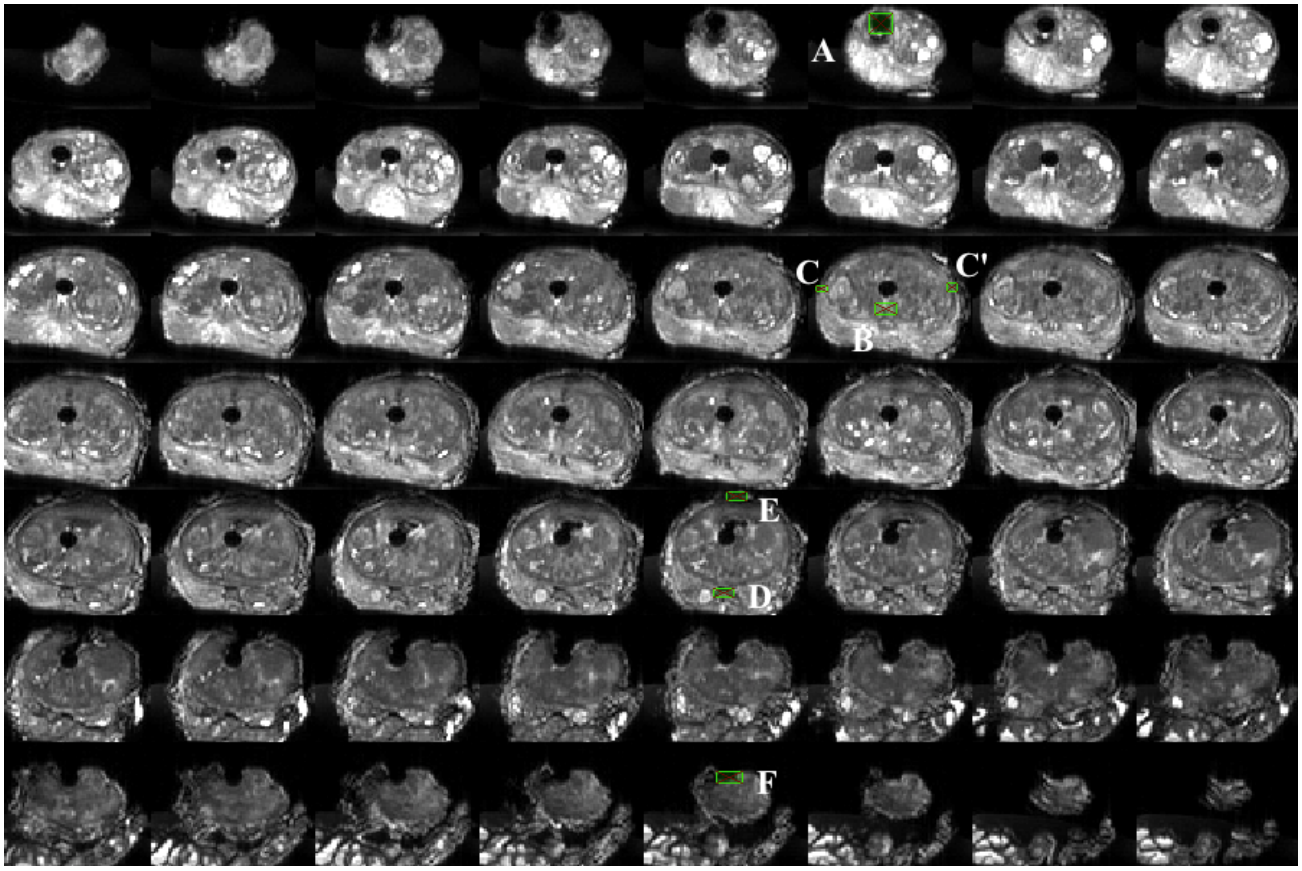

Figure 3. ex vivo MRI-Matching Landmarks with surgical specimen for co-registration –axial plan

Each landmark is specified with its *x,y,z* coordinate values and its name. The operator labels the matching landmarks P_i and Q_i. i=1….n. with the same name across modalities. The software provides an option to graphically move the landmark on the image for fine-tuning of its location and for saving the entire set to a file. The operator then decides on the direction of the transformation by identifying the source volume (moved image) and the target volume (still image).

Given two lists of *n* landmarks. one $P = \{P_1. P_2. \ldots .P_n\}$ on the source volume. and another $Q = \{ Q_1. Q_2. \ldots .Q_n\}$ for the target volume, we compute directly the rigid and the affine transformation T which minimizes the Frobenious norm of the matric $\| T(P) - Q \|$. The computation is based on known analytical solutions [171819].

The residual errors are computed for each landmark and the overall residual root mean square (RMS) distance is computed and recorded. After computing the transformation, three common types of image interpolation are implemented: the nearest neighbor, tri-linear, and sinc interpolation. The RMS across corresponding control points was used to assess co-registration error. Coregistration accuracy was confirmed by multi-modality viewing using operator-guided variable transparency.

2.8. Data analysis

We compared the performance of the rigid and affine transformation models using Student T-test for paired data if data follow normal distribution. If not, Wilcoxon signed-rank test for paired data is used. Significant p value threshold is defined at 0.05. R Software (Vienna University, FDA approved. http://www.r-project.org/) is used for statistical analysis.

3. RESULTS

3.1. Rebuilding

We were able to rebuild surgical specimen in all cases. The process results in 3 files in Analyze format. Figures 1-3 illustrate rebuilt 3D prostate for a representative case. In particular, sagitally reformatted view of the specimen shown in Figure 2 demonstrates successful linear alignment of the urethra and posterior capsule.

3.2. Patient characteristics and pathology results:

Patient age ranges from 54 to 72. The PSA levels are 5.1-7.7ng/ml. Two specimens were pT3a and one pT2b (negative margin) at pathology.

3.3. Transformation and Registration accuracy

The software successfully fused in-vivo T2W MRI. ex-vivo MRI fresh specimen. rebuilt surgical specimen and histology using appropriate (rigid and affine) transformation models. Figure 3 depicts the workflow used for registration.

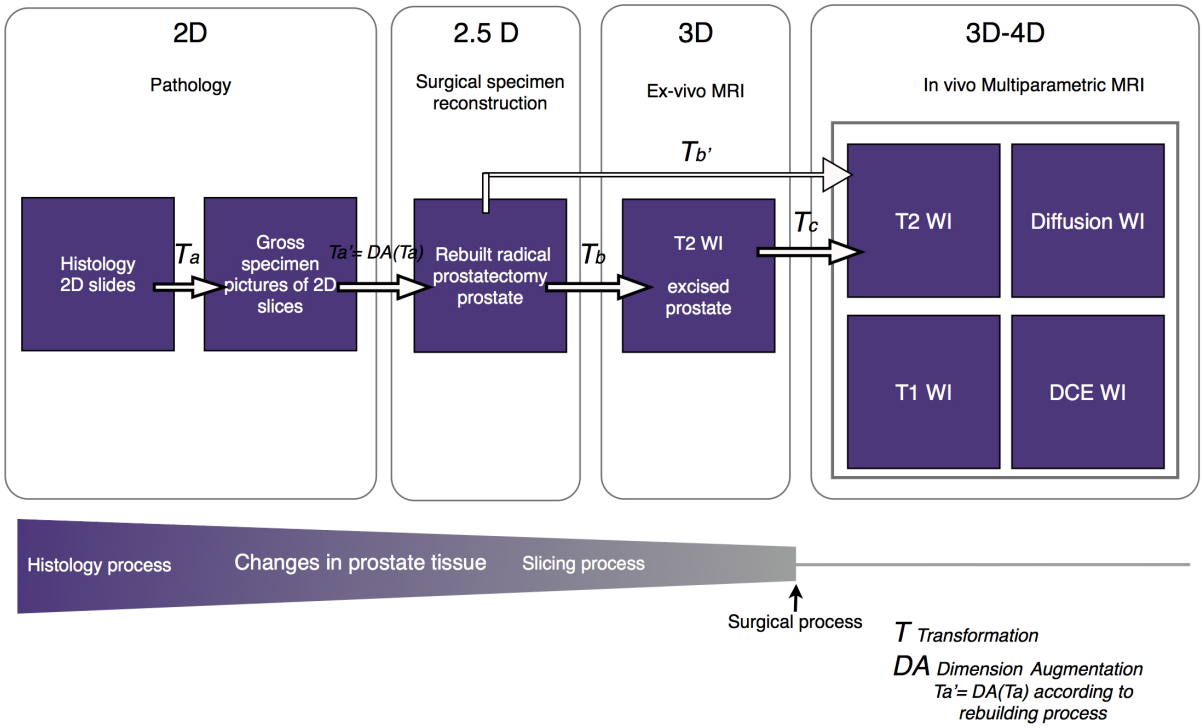

Figure 3 Coregistration workflow

The accuracy results regarding the distribution of RMSE are listed in tables 1 and 2. It is seen that affine transformation performs registration with better accuracy for ex-vivo MRI to in-vivo MRI and for Specimen to in vivo MRI than rigid transformation, with significant p-value using Student test. Data normality distribution was checked before doing this analysis.

We didn't find significant difference between affine and rigid transformation for Specimen to ex vivo MRI.

Table 1. Average Root Mean Square Error (RMSE) in mm for each transformation (source-target).

	Tb Specimen-T2-exvivo MR		*Tc* T2-exviv-T2-invivo		*Tb'* Specimen-T2 invivo		*Ta* Specimen-pathology average	
	Affine	Rigid	Affine	Rigid	Affine	Rigid	Affine	Rigid
Case 1	2.37	2.82	3.36	3.91	1.87	2.38	0.8	1.9
Case 2	2.94	4.55	3.74	4.5	1.67	2.75	0.7	2.1
Case 3	2.96	4.16	3.42	3.8	1.23	2.44	1.2	2.3
Mean	2.75	3.84	3.5	4.07	1.59	2.89	0.9	2.1
p value affine vs rigid	0.25 (not signif)		**0.03**		**0.04**		**0.006**	
p value *Tc* affine vs *Tb'* affine			**0.01**					

There is two ways to transfer data from the surgical specimen to in vivo MRI: using or not ex-vivo MRI as a link between modality. Table 2 present accuracy of such process.

Table 2. RMSE and comparison for the more accurate transformation to transfer cancer from reported to gross slices histology to in vivo T2 MRI.

	Affine registration		**Rigid registration**	
	RMSE *T b+ Tc*	RMSE *T b'*	RMSE *T b+T c*	RMSE *T b'*
Case 1	5.73	1.87	6.73	2.38
Case 2	6.68	1.67	9.05	2.75
Case 3	6.38	1.23	7.96	2.44
Mean	6.26	1.59	7.91	2.89
p value to *T b'* affine	**0.008**	-	**0.014**	**0.049**

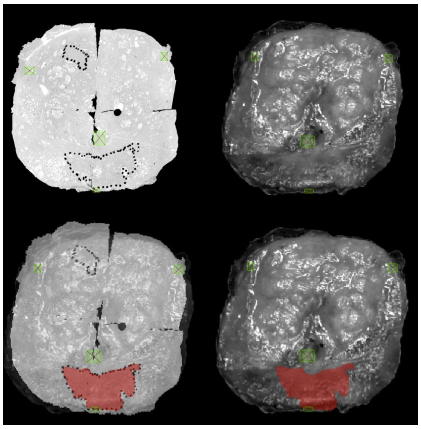

Figure 4. Affine Registration of 2D histology slides on matching specimen slice within 3D rebuilt surgical specimen. Transfer of cancer focus using the same transformation.

3.4. Visualization:

The operator confirmed the consistency of each transformation by modifying the transparency of either source or target after registration. The reliability is confirmed in all transformations. This means that the operator considered the overlap between 2 modalities relevant. Figure 5 illustrates in vivo T2 MRI fused with surgical specimen and evaluation process using transparency.

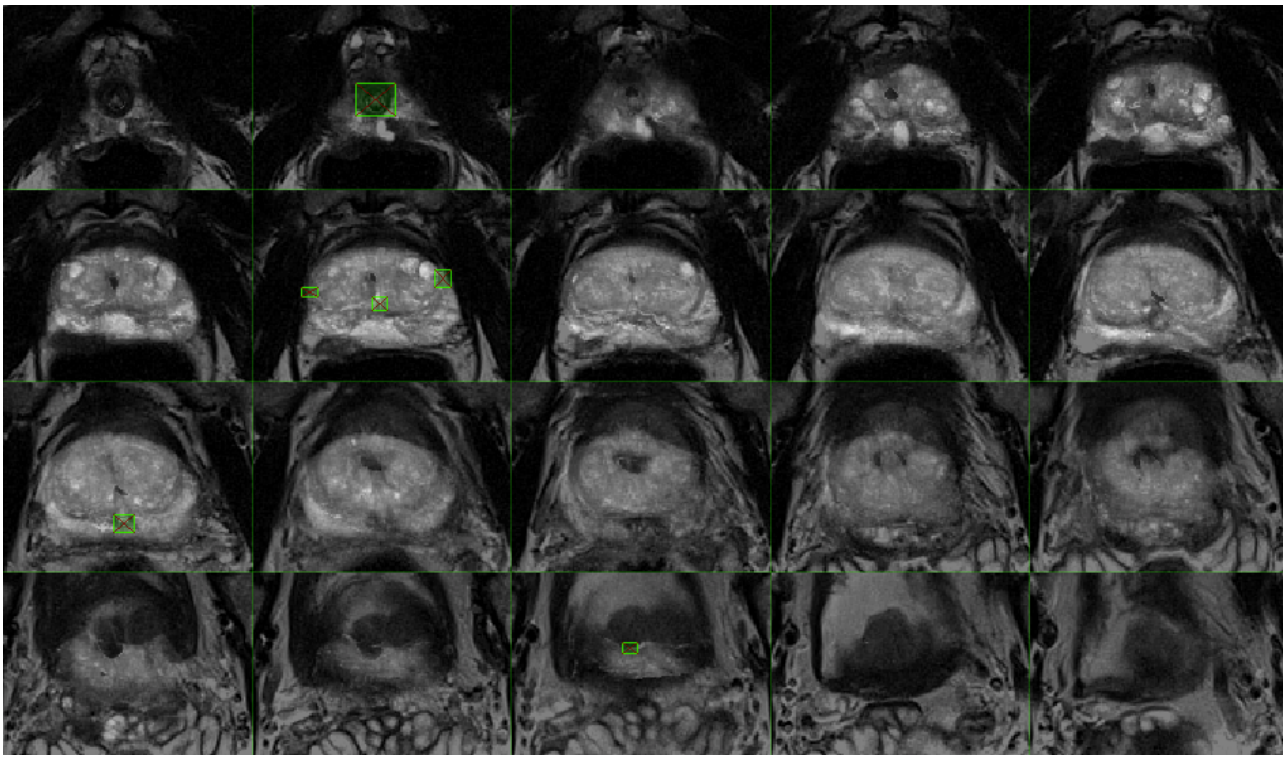

Figure 5. Surgical specimen (source) fused on in vivo T2 MRI (target)-Affine registration

4. DISCUSSION

Until recently validation of MRI findings of lesions suspicious for prostate cancer depended on a subjective. visual approach to correlate in-vivo images with histopathology [2]. A recent study of Mazaheri et al. [12]demonstrated how to automate this process with deformable 2D image co-registration. However. pathologic slices were still pre-matched by a radiologist who selected the corresponding axial T2w images according to their level in the prostate. Qualitative visual matching is important because human expert is capable to guide the process by integrating diverse factors, such as the relative cross-sectional size and shape of the prostate on both modalities, the extent of the peripheral zone and the presence of the transition zone. However, visual matching is limited by inter-observer and intra-observer variability and the lack of quantitative assessment of errors associated with this process.

Physical changes of the prostate due to surgical excision and histology processing steps appear to be a major obstacle to accurate registration. After surgical resection, ex-vivo prostate slices undergo deformation due to mechanical distortions and volume reduction due to dehydration and blood loss. Researchers attempted to overcome the problem by designing dedicated molds for slicing the prostate specimen [2021]. However, it is unlikely that rigid mold will totally eliminate the problem of biomechanical deformation [22]. One way to overcome the problem is to work on 3D representation of ex-vivo specimen that is combined with 3D transformation to fuse in-vivo and ex-vivo data.

This work establishes a framework for co-registration between prostate mpMRI and prostate histology that is objective, Reproducible, and likely to have a good inter-observer reliability. The challenge of combining ex vivo and in vivo modalities is achieved by building successive bridges between 2D and 3D representations. The key step is rebuilding the 3D surgical specimen based on urethra path and rectal wall plane. Any change in volume and slice thickness between MRI and histology can be then corrected with affine transformation that incorporate anisotropic stretching and sheering to account for tissue shrinkage and displacement.

After performing the image fusion, information about any part of the gland, such as a cancer focus, can be transferred across modalities, thus providing researchers with valuable information about the significance of mpMRI features.

In this work. parameters for each transformation are known and recorded. These transformations depend only on robust anatomic landmarks derived from zonal anatomy. They don't rely on the location of cancer foci. The resulting co-registration is capable of transferring arbitrary points and tissue regions from one modality to another in an objective manner. The transformation direction is reversible, i.e., by switching the order of files one can map from histology to MRI and from MRI to histology. Anatomic landmarks extracted from zonal anatomy are already utilized in MRI guided interventions such as biopsy [23]. It is important to evaluate the registration accuracy for such method. as misplacement error crucial in evaluating surgical planning and focal therapies.

In our study we have observed an average error of 1.59 mm for mapping in vivo MRI to surgical specimen. The mean error of 1.59 mm appears to be acceptable, as clinically significant cancer site is defined as being larger than 7 mm (19). Our errors are consistent with the results of Park et al [18] that report 3.7 mm registration errors when fusing diffusion MRI and histology. However, the analysis employed by Park is limited by assuming a perfect inter-modality agreement. In [18] errors were estimated by matching histologically proven cancer lesions with the sites of low ADC value.

Our results indicate that affine transformation is superior over the rigid transformation for aligning in-vivo with ex-vivo image of the prostate. This result indirectly demonstrates that volume changes. The volume decrease after surgical removal of a mean of 4.96 cc related to a mean volume of 43.9 cc for the in vivo MRI. The 10% volume change occurs in the process of surgical extraction.

Twelve degrees of freedom appears to be the minimum required for accurate modeling of the surgical removal and histology processing. However, visual inspection suggests that affine transformation is insufficient for accurate tissue analysis, including glandular density, percentage of loose stroma and the ratio of malignant to benign stromal lesions. More sophisticated deformation models based on significantly higher degree of freedom is the subject of active research that will no doubt improve future studies of inter-modality co-registration of prostate images.

Our method for 3D assembly of a surgical model is important in future studies validating focal therapies for prostate cancer. Our method could compare the boundaries of the target derived from MRI findings against the surgical model. This is important because surgically excised tissue is not yet deformed by the histology processing. Currently there is no other validation technique to assessment accurate localization of focally destroyed tissue [24252627].

Our workflow is attractive because it allows a direct coregistration between pathology and in vivo MRI, without the need of an intermediate image representing ex-vivo MRI. Our experiments demonstrate that combining the two transformations (1) in vivo MRI -> ex-vivo MRI and (2) ex-vivo MRI -> pathology gives no advantage over coregistering in vivo MRI with pathology. This is an important finding because building 3D ex vivo MRI volume is an elaborate and time consuming process.

One way to improve the current workflow would be to incorporate a more powerful deformable transformation such as the polynomial transformation model or the multi-grid algorithm that reflects physical properties of the prostate. Such a transformation would be especially important for prostate MRI performed with an endorectal coil.

A limitation of our workflow is the need of an expert observer to delineate corresponding anatomic landmarks. Voxel-based similarity measures such as mutual information have been validated by others, but these methods are currently limited to 2D images [13]. Another limitation is the use of linear displacement to express the accuracy of coregistration. Other useful measure not tried in present study is the overlap between substructures. Finally, processing of histologic slides could be potentially improved by the use of dedicated whole-mount scan. However, whole-mount technique is costly as it involves purchasing specialized equipment, special blocks and large cassettes for the storage of whole mount sections during processing. The current approach is software based and doesn't require expensive equipment. This feature is important for wider application of our method, including its use multi-center trials.

In conclusion, we have established and validated a workflow for co-registration between pre-operative prostate MRI and pathology with clinically acceptable accuracy. The system is able to account for change in specimen volume due to dehydration and blood loss. Our initial results support the use of our framework for MRI-guided surgical planning and focal therapies. Further improvement will be achieved with the use of higher-order deformable algorithms.

REFERENCES

[1] Dickinson, L., Ahmed, H.U., Allen, C., Barentsz, J.O., Carey, B., Futterer, J.J., Heijmink, S.W., Hoskin, P.J., Kirkham, A., et al., "Magnetic resonance imaging for the detection, localisation, and characterisation of prostate cancer: recommendations from a European consensus meeting," European Urology 59(4), 477-494 (2011).

[2] Villers, A., Puech, P., Mouton, D., Leroy, X., Ballereau, C., and Lemaitre, L., "Dynamic Contrast Enhanced, Pelvic Phased Array Magnetic Resonance Imaging of Localized Prostate Cancer for Predicting Tumor Volume: Correlation With Radical Prostatectomy Findings," The Journal of Urology 176(6), 2432-2437 (2006).

[3] Hoeks, C.M.A., Barentsz, J.O., Hambrock, T., Yakar, D., Somford, D.M., Heijmink, S.W.T.P.J., Scheenen, T.W.J., Vos, P.C., Huisman, H., et al., "Prostate Cancer: Multiparametric MR Imaging for Detection, Localization, and Staging," Radiology 261(1), 46-66 (2011).

[4] Turkbey, B., Mani, H., Shah, V., Rastinehad, A.R., Bernardo, M., Pohida, T., Pang, Y., Daar, D., Benjamin, C., et al., "Multiparametric 3T prostate magnetic resonance imaging to detect cancer: histopathological correlation using prostatectomy specimens processed in customized magnetic resonance imaging based molds," The Journal of Urology 186(5), 1818-1824 (2011).

[5] Rosenkrantz, A.B., Scionti, S.M., Mendrinos, S., and Taneja, S.S., "Role of MRI in minimally invasive focal ablative therapy for prostate cancer," AJR. American Journal of Roentgenology 197(1), W90-96 (2011).

[6] Taneja, S.S., and Mason, M., "Candidate selection for prostate cancer focal therapy," Journal of Endourology / Endourological Society 24(5), 835-841 (2010).

[7] Tareen, B., Godoy, G., and Taneja, S.S., "Focal therapy: a new paradigm for the treatment of prostate cancer," Reviews in Urology 11(4), 203-212 (2009).

[8] Freedland, S.J., Partin, A.W., Humphreys, E.B., Mangold, L.A., and Walsh, P.C., "Radical prostatectomy for clinical stage T3a disease," Cancer 109(7), 1273-1278 (2007).

[9] Jonmarker, S., Valdman, A., Lindberg, A., Hellström, M., and Egevad, L., "Tissue shrinkage after fixation with formalin injection of prostatectomy specimens," Virchows Archiv 449(3), 297-301 (2006).
[10] Schned, A.R., Wheeler, K.J., Hodorowski, C.A., Heaney, J.A., Ernstoff, M.S., Amdur, R.J., and Harris, R.D., "Tissue-shrinkage correction factor in the calculation of prostate cancer volume," The American Journal of Surgical Pathology 20(12), 1501-1506 (1996).
[11] Chen, L.H., Ho, H., Lazaro, R., Thng, C.H., Yuen, J., Ng, W.S., and Cheng, C., "Optimum slicing of radical prostatectomy specimens for correlation between histopathology and medical images," International Journal of Computer Assisted Radiology and Surgery 5(5), 471-487 (2010).
[12] Mazaheri, Y., Bokacheva, L., Kroon, D.-J., Akin, O., Hricak, H., Chamudot, D., Fine, S., and Koutcher, J.A., "Semi-automatic deformable registration of prostate MR images to pathological slices," Journal of Magnetic Resonance Imaging 32(5), 1149-1157 (2010).
[13] Chappelow, J., and Madabhushi, A., "Multi-attribute combined mutual information (MACMI): An image registration framework for leveraging multiple data channels," in 2010 IEEE International Symposium on Biomedical Imaging: From Nano to Macro, 376-379 (2010).
[14] Xiao, G., Bloch, B.N., Chappelow, J., Genega, E.M., Rofsky, N.M., Lenkinski, R.E., Tomaszewski, J., Feldman, M.D., Rosen, M., et al., "Determining histology-MRI slice correspondences for defining MRI-based disease signatures of prostate cancer," Computerized Medical Imaging and Graphics: The Official Journal of the Computerized Medical Imaging Society 35(7-8), 568-578 (2011).
[15] Noguchi, M., Stamey, T.A., McNeal, J.E., and Yemoto, C.E., "Assessment of morphometric measurements of prostate carcinoma volume," Cancer 89(5), 1056-1064 (2000).
[16] McNeal, J.E., "Normal histology of the prostate," The American Journal of Surgical Pathology 12(8), 619-633 (1988).
[17] Golub, G.H., and Van Loan, C.F., [Matrix computations] , Johns Hopkins University Press, Baltimore (1996).
[18] Dryden, I.L., and Mardia, K.V., [Statistical shape analysis] , John Wiley & Sons, Chichester; New York (1998).
[19] Fitzpatrick, J.M., West, J.B., and Maurer, C.R., Jr, "Predicting error in rigid-body point-based registration," IEEE Transactions on Medical Imaging 17(5), 694-702 (1998).
[20] Turkbey, B., Mani, H., Shah, V., Rastinehad, A.R., Bernardo, M., Pohida, T., Pang, Y., Daar, D., Benjamin, C., et al., "Multiparametric 3T Prostate Magnetic Resonance Imaging to Detect Cancer: Histopathological Correlation Using Prostatectomy Specimens Processed in Customized Magnetic Resonance Imaging Based Molds," The Journal of Urology 186(5), 1818-1824 (2011).
[21] Trivedi, H., Turkbey, B., Rastinehad, A.R., Benjamin, C.J., Bernardo, M., Pohida, T., Shah, V., Merino, M.J., Wood, B.J., et al., "Use of patient-specific MRI-based prostate mold for validation of multiparametric MRI in localization of prostate cancer," Urology 79(1), 233-239 (2012).
[22] Krouskop, T.A., Wheeler, T.M., Kallel, F., Garra, B.S., and Hall, T., "Elastic moduli of breast and prostate tissues under compression," Ultrasonic Imaging 20(4), 260-274 (1998).
[23] Ouzzane, A., Puech, P., Lemaitre, L., Leroy, X., Nevoux, P., Betrouni, N., Haber, G.-P., and Villers, A., "Combined multiparametric MRI and targeted biopsies improve anterior prostate cancer detection, staging, and grading," Urology 78(6), 1356-1362 (2011).
[24] Taneja, S.S., and Tareen, B., "Targeting prostate cancer for focal destruction: can we find it?," Cancer 113(7), 1500-1501 (2008).
[25] Villers, A., Lemaitre, L., Haffner, J., and Puech, P., "Current status of MRI for the diagnosis, staging and prognosis of prostate cancer: implications for focal therapy and active surveillance," Current Opinion in Urology 19(3), 274-282 (2009).
[26] Sciarra, A., Barentsz, J., Bjartell, A., Eastham, J., Hricak, H., Panebianco, V., and Witjes, J.A., "Advances in magnetic resonance imaging: how they are changing the management of prostate cancer," European Urology 59(6), 962-977 (2011).
[27] Ukimura, O., Faber, K., and Gill, I.S., "Intraprostatic targeting," Current Opinion in Urology 22(2), 97-103 (2012).